Water Quality Research Journal

Water Quality Research Journal Vol 58 No 1, 1 doi: 10.2166/wqrj.2023.010

Measuring nitrate concentration in surface waters with a microfluidic device facilitated by a miniaturized capacitive deionization cell

Hang Zhang[a,b], Ran Zhao[a,c,b,*], Ying Yang[a], Yingwei Liu[c] and Linchen Han[c]

[a] Engineering Research Center for Nanophotonics & Advanced Instrument, Ministry of Education, School of Physics and Electronic Science, East China Normal University, 500 Dongchuan Road, 200241 Shanghai, China
[b] East China Normal University-University of Alberta Joint Institute of Advanced Science and Technology, 3663 North Zhongshan Road, 200062 Shanghai, China
[c] Hangzhou Haoli Technology Co., Ltd, 615 Binfen Street, Hangzhou 310000, China
*Corresponding author. E-mail: rzhao@haolitech.com

ABSTRACT

Excessive nitrate in surface waters poses a great threat to the health of human beings. Traditional measuring tools require either hazardous chemicals or organic matter compensation. In this work, we proposed an online microfluidic device incorporated with a miniaturized capacitive deionization cell that separates organic matter and nitrate ions before the measurement and afterwards determines the nitrate concentration with a 235-nm LED. The optimal operational parameter setting, which is a combination of 600-s charging duration and 0.5-V cell potential, was also obtained in order to achieve the maximum fractionation of nitrate ions. Promising results were obtained by our new approach, revealing that this device could serve as a functional and effective tool for the determination of nitrate concentration in surface water.

Key words: membrane capacitive deionization, microfluidics, nitrate detection, UV spectroscopy

HIGHLIGHTS

- A microfluidic device measures nitrate concentration online.
- The device is composed of a membrane capacitive deionization (MCDI) unit and a detection unit.
- The MCDI unit separates the inorganic ions from the surface water that contains natural organic matter.
- The performance of the device is better than the lab-analyzed results by Chinese national standards with regard to accuracy.

1. INTRODUCTION

Nitrate is one of the primary anthropogenic pollutants in surface waters. The increase of nitrate ions in surface waters in many places of the world is seasonal and tightly related to the use of nitrogen fertilizer for agricultural purposes (Yu *et al.* 2020). Most of the time, the concentration of nitrate in the surface water and groundwater supplies remains at a low level. For instance, in the US, it is normally below 4 mg/L. However, a peak concentration of over 1,500 mg/L has been reported in the agricultural area in India (Cotruvo *et al.* 2011). Nitrate is the key macronutrient that causes eutrophication in natural water (Burt *et al.* 2010) and it also poses a threat to the health of human beings. As natural waters are important drinking water sources, the changes of the nitrate concentration in surface water, e.g. sewage effluent discharge, reflect the exposure of higher nitrate levels in the drinking water. Previous studies have shown that high nitrate concentrations in the drinking water play a significant role in the occurrence of methemoglobinemia in infants exclusively under the age of 3 months (Cotruvo *et al.* 2011). Therefore, monitoring nitrate concentration in natural waters is important for the prediction of pollution accidents, e.g. algal blooms and for safeguarding our drinking water sources.

Traditionally, there are many ways of measuring nitrate in surface waters, including chemistry (Moorcroft *et al.* 2001), electrochemistry (Kaniansky *et al.* 1994; Davis *et al.* 2000), chemiluminescence (Aoki *et al.* 1997), as well as chromatography. The most adopted is the 'wet chemical method', which uses Cr or VCl_3 to reduce all nitrate into nitrite and subsequently reacts with the Griess solution to form a pink solution (Gal *et al.* 2004; Cogan *et al.* 2013). The absorbance of the pink solution at 525 nm light is normally utilized to quantify the strength of the color, which has a linear relationship vs. nitrate concentration over a wide concentration range. Previous researchers have successfully miniaturized this concept using

state-of-the-art microfluidics technology (Beaton *et al.* 2012; Nightingale *et al.* 2019). However, the 'wet chemical' method uses toxic chemicals that might cause secondary pollution to the environment without careful handling and post-treatment. Nitrate and nitrite have very strong responses to ultraviolet (UV) light with a wavelength of 220 nm and also in natural water nitrite concentration is quite low compared to nitrate, the alternative is to measure nitrate with the UV absorption method (National Environmental Protection Bureau (NEPB) 2007; Baird *et al.* 2017). This UV220 method requires the compensation of the UV absorption of the natural organic matter (NOM) at wavelength of 275 nm. This is because the NOM has responses at both 220 and 275 nm, while at 275 nm no response of nitrate is found. This method is much more direct and speedy than the 'wet chemical' method. Therefore, it is adopted by many countries for the fast analysis of nitrate ions in aqueous solutions. However, if we want to transplant this method to the framework of microfluidics, at the present, the size of the luminous gas source is the greatest hindrance.

Fortunately, nitrate does not only respond to UV light at 220 nm, specifically. Its responding region of UV light extends up to 240 nm, although the response decays along with the increase of UV wavelength (Supplementary information). To be specific, the strength of the responding signal measured by a spectrophotometer of a fixed nitrate concentration at a wavelength of 235 nm is only about one-tenth the signal measured at a wavelength of 220 nm. Because of the much weaker signal level compared to wavelength of 220 nm, it is then very important to keep the UV absorption signal from the disturbance of the organic matter. As in the surface waters, the majority of the NOMs are humic acid and fulvic acid (Rodrigues *et al.* 2009; Costa *et al.* 2011). Previous studies have shown that the molecular weights of these organic compounds are larger than 100 g/mol (MacFarlane 1978; Thurman *et al.* 1982; Klučáková 2018). Taking advantage of these properties, we have fabricated a miniaturized capacitive deionization (CDI) cell with monovalent exchange membranes with the cutoff molecular weight of 100 g/mol in order to separate the monovalent ions, including nitrate from the surface water samples, which contain NOMs, in other words, the chemical oxygen demand (COD). The miniaturized membrane capacitive deionization (MCDI) module was then coupled to a microfluidic device incorporating an UV-235 nm LED in order to measure the surface water samples without the interference of the NOMs.

MCDI is the modified form of CDI, which has been emerging as a desalination technology in recent years (Porada *et al.* 2013). A typical MCDI cell consists of two porous electrodes, which are normally fabricated by carbon materials, e.g. activated carbon, graphene, carbon nanotubes, and recently there are lots of attempts to achieve greater salt adsorption by using novel materials (Noonan *et al.* 2018; Divyapriya *et al.* 2019; Ma *et al.* 2020; Peng *et al.* 2020; Xu *et al.* 2020; Li *et al.* 2021). On the surface of each electrode, an ion-exchange membrane is attached (anion exchange membrane on the anode; cation exchange membrane on the cathode). A spacer channel is between the two membranes, which allows the water to flow through. When an electrical voltage is applied to the cell, the ions in the spacer channel will be absorbed into their counter electrodes, thereby the water is deionized. Recently, there have been many attempts to use CDI or MCDI to selectively remove a certain ion from a mixture of ions, either with the pore size, the electrode's affinity to certain ions or the ion's diffusion coefficient (Mubita *et al.* 2019; Cerón *et al.* 2020; Hong *et al.* 2020). In this work, we employed the monovalent anion membranes, which were capable of retaining most organic matter and divalent anions in the spacer channel, while absorbing nearly all nitrate ions.

2. EXPERIMENTAL SECTION

2.1. Materials

All chemicals are of analytical reagent grade and used without further purification. Polyvinylidene fluoride (PVDF) was supplied by Shanghai New Materials Co., Ltd (China). The graphite plates purchased from Baofeng Graphite Ltd (Shangdong, China). Activated carbon powders are made from coconut shell (YP-50, Kuraray, Japan). N-methyl-2-pyrrolidone (NMP) and sodium chloride (NaCl) were purchased from Sinopharm Chemical Reagent Co., Ltd. The monovalent anion exchange membrane (ACS, 0.13 mm) and the monovalent cation exchange membrane (CIMS, 0.15 mm) were supplied by Astom Corporation (Tokyo, Japan). The cutoff molecular weights of the two membranes are 100 Da, according to the technicians from the supplier. Before use, the membranes were soaked in a 0.1 M NaCl for 24 h. All surface water samples in this work were prefiltered with a 0.45 mm filter and the installation by the river has a pretreatment of a microfiltration membrane with a pore size of 0.1 mm. Diluted NaCl solution (10 mM) was used to clean the system and was used as the electrolyte during the discharging step.

2.2. The MCDI electrode module

The MCDI module has a symmetrical structure. It has two titanium current collectors embracing two graphite plates. On the inner side of each graphite plate's surface, there is a layer of coated activated carbon electrode that was used for ion adsorption. To make the electrode, PVDF (previously dissolved in NMP, 1:30) and carbon black powder were mixed at a ratio of 1:9 to obtain a homogeneous slurry, and then it was coated onto the graphite plates (oval shaped for better hydrodynamics; area = 1,321 mm^2). The graphite plates were then dried at 80 °C for 10 h. After drying, the final thickness of the obtained electrode is 250 μm and the activated carbon electrode has a pore volume of 0.6 cm^3/g, and a surface area of 1,156 m^2/g Brunauer Emmett Teller (BET) area, measured by the nitrogen adsorption method).

The monovalent anion exchange membrane is placed on the surface of the positive electrode and likewise, the monovalent cation exchange membrane is placed on the surface of the negative electrode. Two sealing gaskets are located on an annular groove of both graphite plates surrounding the electrode area to prevent any side leakage. After assembly, the hollow space of the mid-plate becomes the spacer channel and the thickness is 0.8 mm, resulting in the final spacer channel's volume of 1 mL. Two fluid orifices on one outer plate (right, Figure 1(b)) are configured to connect two orifices on the mid-plate that are channeled to the spacer channel through the bended microfluid paths in the body of the mid-plate (indicated in Figure 1(a)).

2.3. The microfluidic chip including the detection module

The microfluidic platform based on a rectangular block of polymethylmethacrylate (PMMA) has a dimension of 6 mm × 13 mm (width × length). This chip was machined in 4 mm thick transparent PMMA plate by a Computer Numerical Control (CNC) machine (DJ450LE, Changzhou Kuaile Science And Technology, Co., Ltd). According to Ogilvie *et al.* (2010), the solvent vapor bonding method was used to bond the two halves of the PMMA to form a complete chip. The microfluidic chip incorporates a fluidic manifold that permits selection of two inlets, the sample and NaCl solution. Fluid control is achieved by using the combination of two one-way pumps, one two-way pump, and five valves, described in Figure 2(a). The system has a 'rocking chair'-like structure, which means that by opening either air valve, we can pump the fluid to the specified flow path, either the MCDI module or the detection module. By opening either air valve or turning on the one-way pump on the other

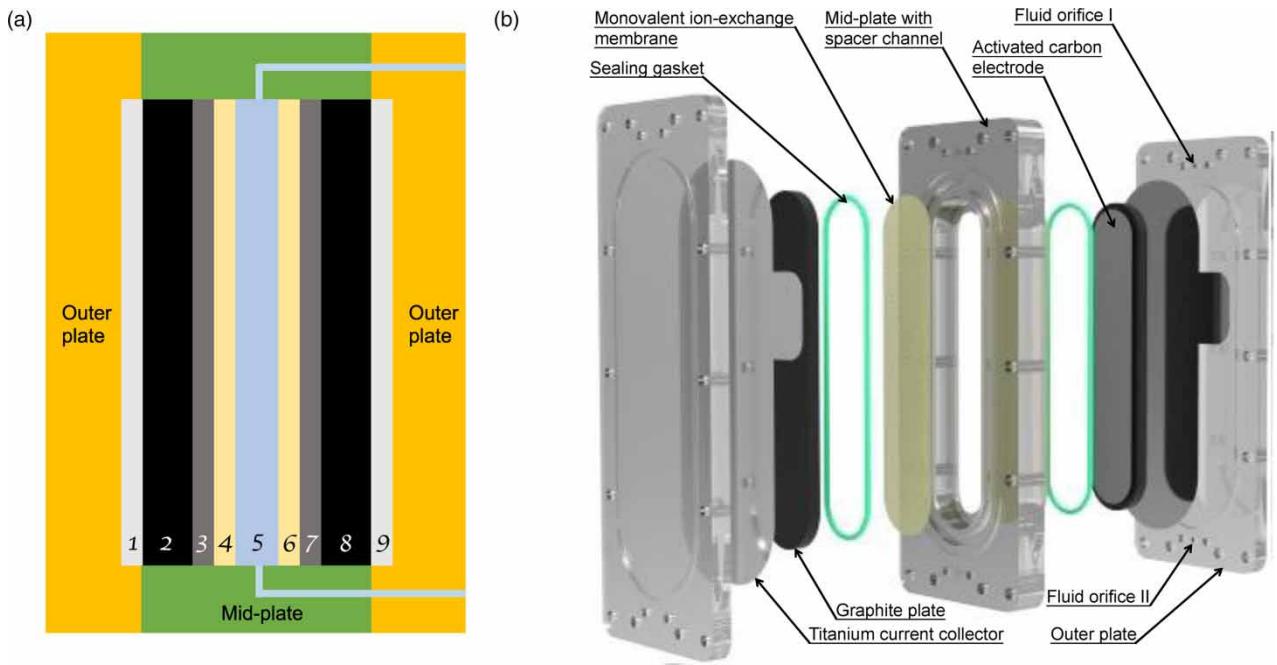

Figure 1 | (a) Schematic view of the MCDI module, including the mid-plate, outer plates, and the core units. Units 1 and 9 are the titanium current collectors, units 2 and 8 are the graphite plates, units 3 and 7 are the activated carbon electrodes, units 4 and 6 are the monovalent anion/cation exchange membranes, and unit 5 is the spacer channel. (b) Explosive view of the components of the MCDI module, including two outer plates, two titanium current collectors, two graphite plates, two sealing gaskets, two activated carbon electrodes, two monovalent ion-exchange membranes, and a mid-plate with spacer channel.

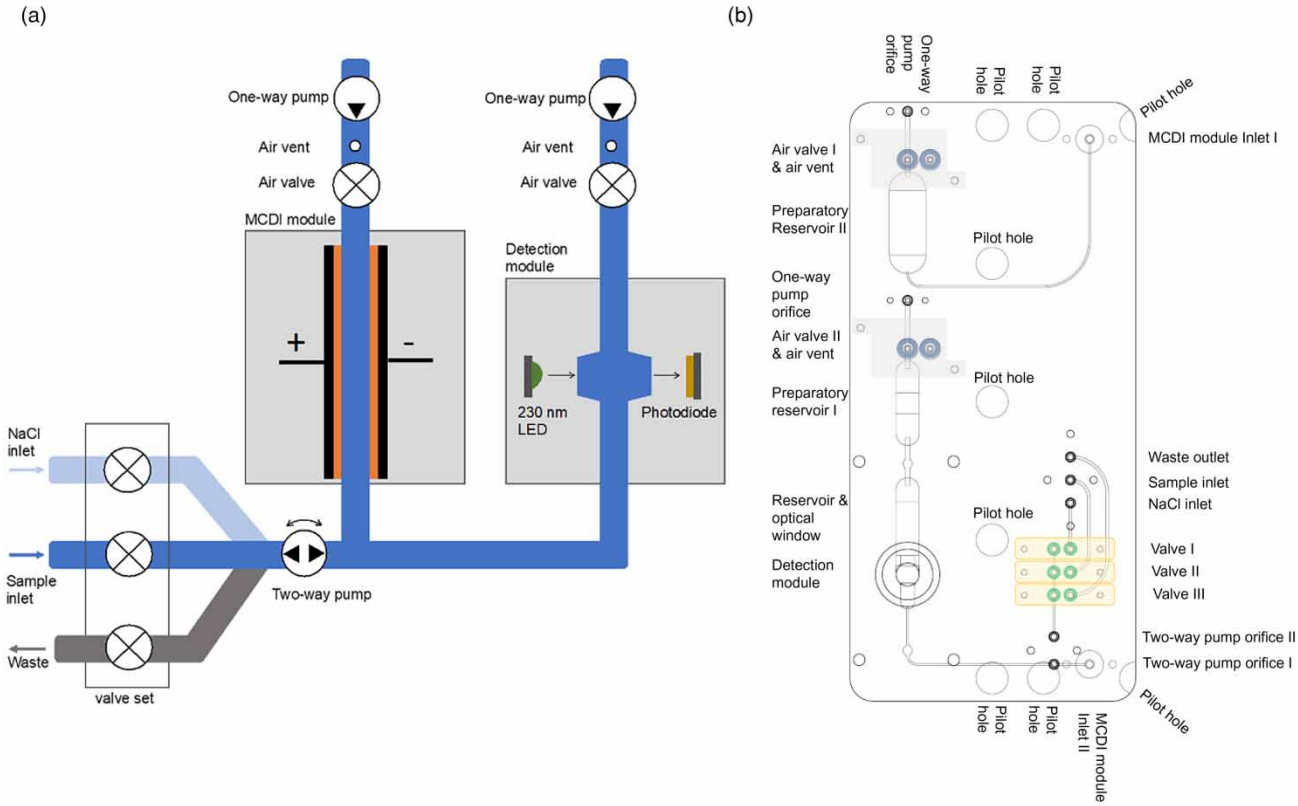

Figure 2 | (a) Fluidic path diagram indicating the flow paths of the device, including two inlets, one waste and the MCDI module, as well as the detection module; and (b) Management Software Computer Aided Design (CAD) drawing of the microfluidic chip with fluidic connections labeled.

flow path, the fluid can be controlled to flow forth and back between the detection module and the MCDI module. The MCDI module is fixed on the surface of the chip, where the two fluid orifices on the MCDI module are aligned and sealed with MCDI module Inlets I and II (Figure 2(b)). Except for the reservoirs and the optical cell in the chip, the microfluidic channels have a uniform square cross section with equal width and depth (both are 0.2 mm).

In the beginning of the whole process, the fluid is firstly pumped into the detection module. A spindle-like optical cell is designed in order to prevent the formation of the dead volume and the disturbance of the air bubbles. The optical cell has a light path of 10 mm, which is specially designed for measuring nitrate in surface water and its volume is 800 mL. The UV-235 nm LED (OP235-nX-SM, Asahi Kasei, Japan) and photodiode (GUVC-T21GH, Genicom, Korea) were fixed on the chip face-to-face by a dismountable bracket, sandwiching the optical cell. After the first absorbance is measured, the sample then flows into the spacer channel of the MCDI module. At the same time, charging starts, which leads to the fast adsorption of the monovalent inorganic ions. After the adsorption process ends, the stream will be transported to the detection module again to measure the absorbance of the 235 nm LED. After the measurement is over, the liquid residual in the detection module will be discharged. NaCl solution will be used to clean the detection chamber and afterwards will be transferred to the MCDI cell, where the voltage is now set to zero and the adsorbed ions will be released, which is the regeneration step. Afterwards, the solution will be discharged and the system will be regenerated.

3. RESULTS AND DISCUSSION

3.1. Concentration response

The concentration response follows the Lambert–Beer law, where a calibration curve is relating the optical absorbance to the concentration of the nitrate ions. However, in the surface water, because of the presence of the organic matter, the absorbance before the separation of the organics and the inorganics refers not only to the nitrate ions but also to the organic

matter, which is the summation of the two components, given by

$$A_{235\text{nm}} = A_{NO_3} + A_{OM} \quad (1)$$

where $A_{235\text{nm}}$ is the optical absorbance at a wavelength of 235 nm, A_{NO_3} is the part contributed by the nitrate ions, and A_{OM} is the part contributed by the organic matters.

Since all the water samples entering our device are prefiltered, the disturbance of the turbidity of the surface water sample is no longer a concern. In our method, the water samples have to be measured twice, before and after the MCDI adsorption. Therefore, the calculation does not need to involve the compensation of a second UV light (275 nm), which is simply the difference of the two measurements ($A_{NO_3} = A_{235\text{nm}} - A_{OM}$). This value will then be taken into the calibration curve to find out the eventual concentration of nitrate.

Changes in the conductivity may be a challenge for the MCDI module to overcome since the porous carbon electrodes we employed here have a limited capacity. Due to previous reports, the capacity of the electrode made by the given recipe is around 9 mg NaCl/g electrode weight (Porada *et al.* n.d.). Because the monovalent membranes used in this work can prevent most divalent ions from entering the electrode region as well as the NOMs, the activated carbon electrodes can be used to adsorb as many monovalent ions as possible.

The limit of detection (LOD) and the limit of quantification were determined to be 0.03 and 0.12 mg/L, respectively, using the three-sigma method, which is mainly determined by the light source, the photodiode as the light signal sensor, the accuracy of the ADC (Analog-to-digital converter) chip on the Printed Circuit Board (PCB) board, and the length of the light path, which is set at 10 mm. The calibration curve (Figure 3) shows a good correlation in the lower range (0–20 mg/L), ($R^2 > 0.999$), and each data point was measured seven times, which shows a very low relative standard deviation (RSD $<$ 0.5%). Therefore, the measuring range of our device is set in the range of 0–20 mg/L nitrate ions, which can suffice the requirement of nitrate detection in surface waters in most cases.

3.2. Optimization of the parameters

Three different surface water samples were examined before and after the adsorption process in order to select the optimal running condition for our device. For each sample, fixed voltages (0.5, 0.8, and 1.1 V) were consecutively applied and the adsorption duration for each water sample was varied for each voltage (300, 600, and 900 s). Before and after the adsorption procedure, the optical absorbance values at 235 and 275 nm were measured by a spectrophotometer (UVmini-1285, Shimadzu, Japan), which represent concentrations of nitrate and NOMs, respectively.

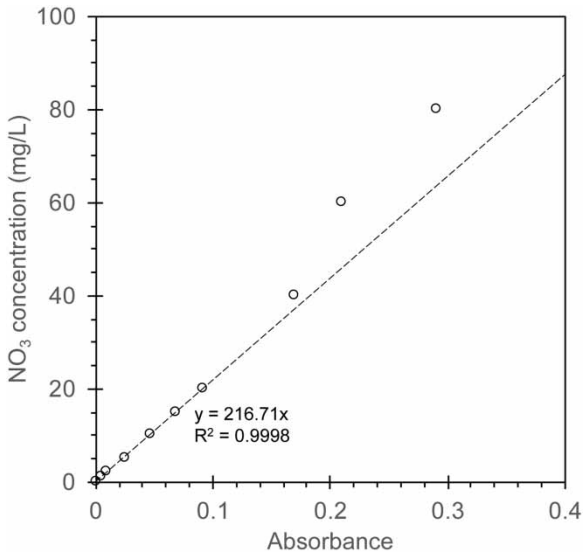

Figure 3 | Nitrate concentration as a function of absorbance. The dotted line is the linear fitting curve for the lower range (0–20 mg/L) generated in Excel, using the data point from 0 to 20 mg/L.

In Figure 4, the three different surface water samples exhibited a certain degree of similarity in that along with the adsorption time, the optical absorbance at 275 nm gradually declined, which represents the change in the concentration of the NOM in the surface water. For the lowest voltage, the declination in the beginning in insignificant, which normally lasts for 800 s, while this rather stable plateau cannot be found in the highest voltage (1.1 V). This phenomenon shows that under lower voltages, the NOMs with charge or the organic ions are penetrating the membrane much slower and in the meanwhile, it is observed a substantial drop at a wavelength of 235 nm, which stands for pure inorganic ion adsorption. Then, a plateau at 235 nm of the data at 0.5 V around 500–600 s can also be observed. During this time span, very little adsorption for either inorganic ion adsorption or organic ion adsorption occurs. After that, the optical absorbance for 235 nm continuously

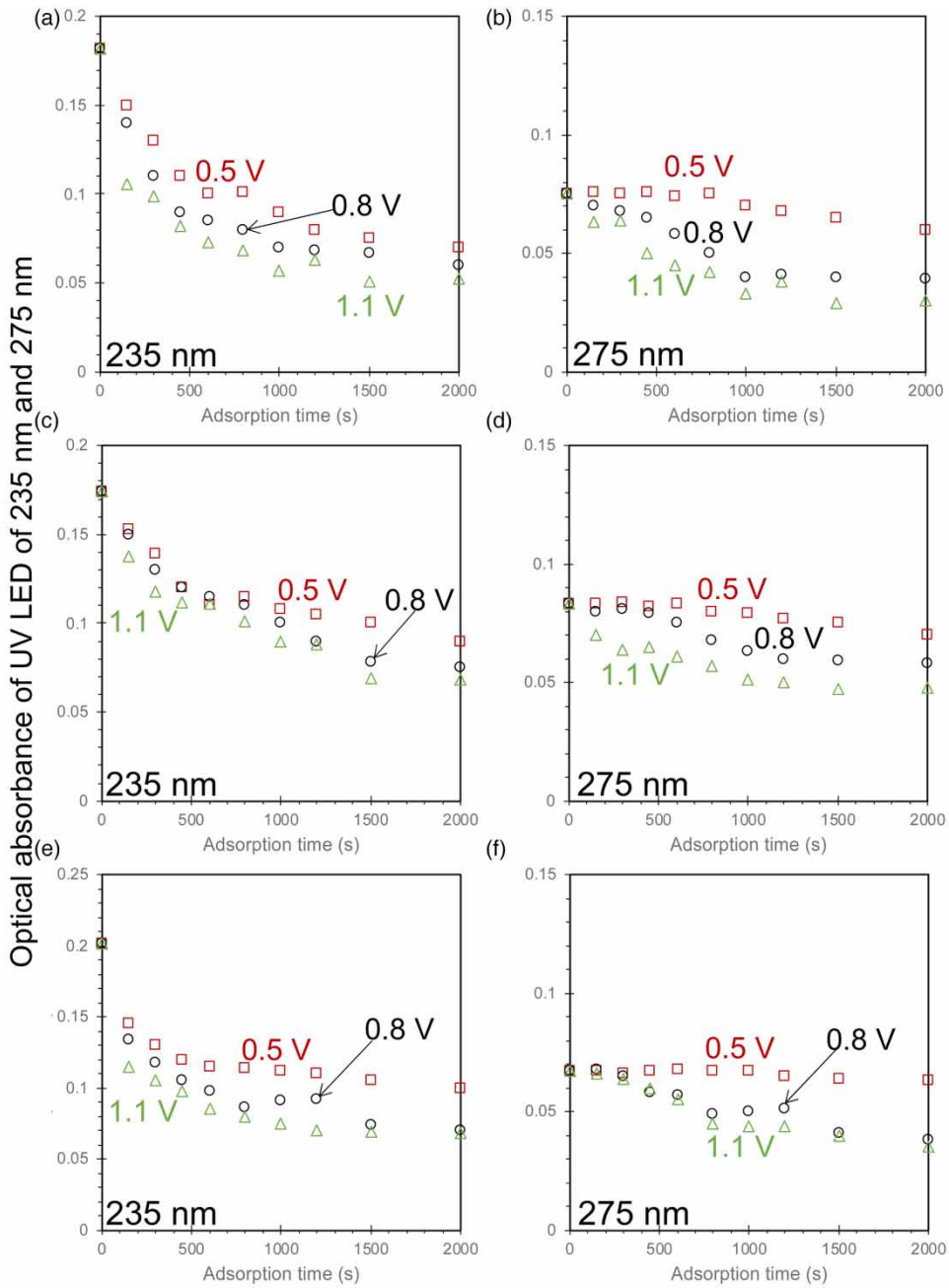

Figure 4 | The optical absorbance of three surface water samples as a function of the adsorption time for different voltages at wavelength of 235 nm (a, c, and e) and 275 nm (b, d, and f). The red squares are experiments with 0.5 V, the black circles are with 0.8 V, and the green triangles are with 1.1 V. Please refer to the online version of this paper to see this figure in color: http://dx.doi.org/10.2166/wqrj.2023.010.

decreases, which mainly attributes to the adsorption of the organic matter. It is suggested that either longer adsorption time or higher adsorption voltage can lead to a breach of the defense against NOMs by the monovalent ion-exchange membrane. Therefore, the combination of 600 s and 0.5 V might be a suitable parameter setting for the MCDI module. Whereas for the lowest voltage (0.5 V), the only concern is whether it can lead to a full adsorption of nitrate ions.

In order to find out if the nitrate ions are fully adsorbed, we analyzed the concentrations of the major anions in 10 water samples before and after the adsorption procedure by ion chromatography (D160, Qingdao Shenghan Chromatograph Technology Co., Ltd, China). The pristine water samples and their respective discharged liquids residual (Step 7) from the standard process (Supplementary information, S3) were taken, under a voltage of 0.5 V for 600 s, and afterwards the effluents were collected while the voltage was still on. Because the volume of the spacer channel of the MCDI module is quite limited (only 800 μL), the experiment for each sample was repeated five times in order to collect enough aqueous sample for ion chromatography. It is demonstrated clearly that the monovalent ions are greatly adsorbed, whereas most divalent ions (sulphate ions) are prevented from entering the porous electrodes structure because of the monovalent ion-exchange membrane (Figures 5(a)–5(c)). The significant concentration decrease of the monovalent ions is the main contribution of the conductivity drop before and after the adsorption (Figure 5(d)) Moreover, the adsorption of the nitrate ions is rather complete. Their concentration decreased by two orders of magnitude (Figure 6(a)).

3.3. Interference of competing ions

The majority of anion species present in the surface water in the Shanghai area consists mainly of Cl^-, NO_3^- and SO_4^{2-} according to the analysis by ion chromatography and the conductivities of most surface waters in this area are below 1,000 μS/cm. Thus, it is necessary to evaluate the interference of ions in regard to their competition with nitrate ions in the adsorption by the porous electrodes. The biggest competitor is chloride ions since they are also monovalent and their concentration in the water samples is much higher compare to nitrate. However, as is previously reported (Mubita *et al.* 2019), the nitrate ions may have an advantage against chloride ions during the adsorption process in the electric double-layers, even if they are at a disadvantage in terms of quantity. A mixture of KNO_3 and NaCl and a mixture of KNO_3 and $MgSO_4$ were tested using the standard process of the device (described in Supplementary information). The ratio of nitrate adsorption was calculated by the two-time measurements by the 235 nm UV LED. During the experiments, the NO_3^- concentration is fixed (8.85 mg/L) and the concentrations of the competing ions are varied between 0 and 500 mg/L.

Figure 3(a) shows that in the beginning the nitrate can sustain a 100% adsorption ratio, but when we continue to increase the background chloride concentrations, finally the adsorption ratio starts to drop at the point that the chloride concentration reaches 240 mg/L, and the respective conductivity is over 1,000 μS/cm. Whereas for the magnesium sulphate as the background ion, the nitrate adsorption is not affected by the increase of the magnesium sulphate concentration. The

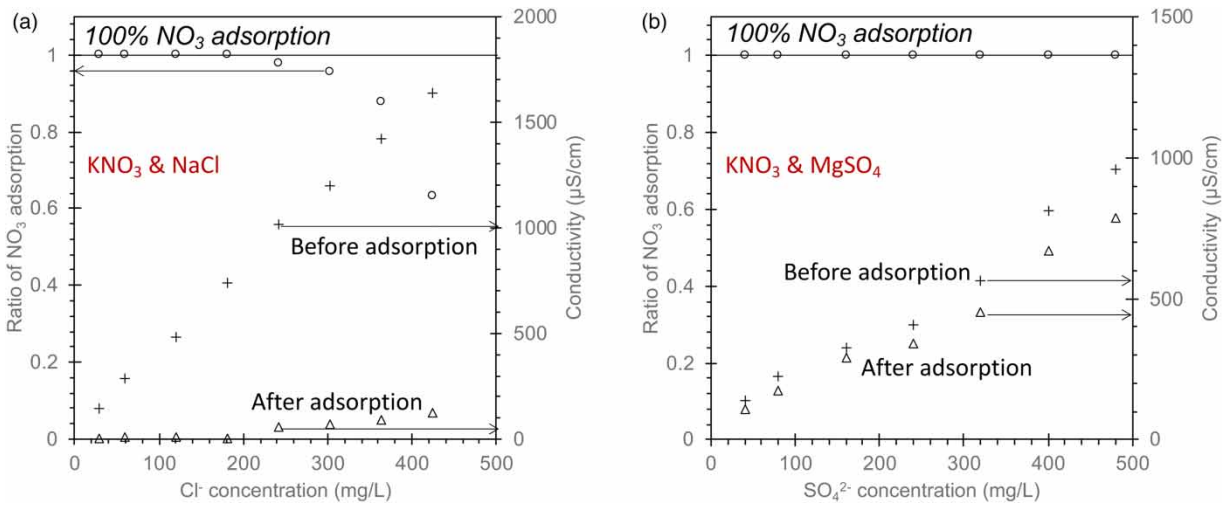

Figure 5 | Ratio of nitrate adsorption and conductivity change as a function of background ion concentration, (a) Chloride; and (b) Sulphate. The NO_3 concentrations in all cases are equal to 8.85 mg/L (equivalent to 2 mg N-NO_3/L).

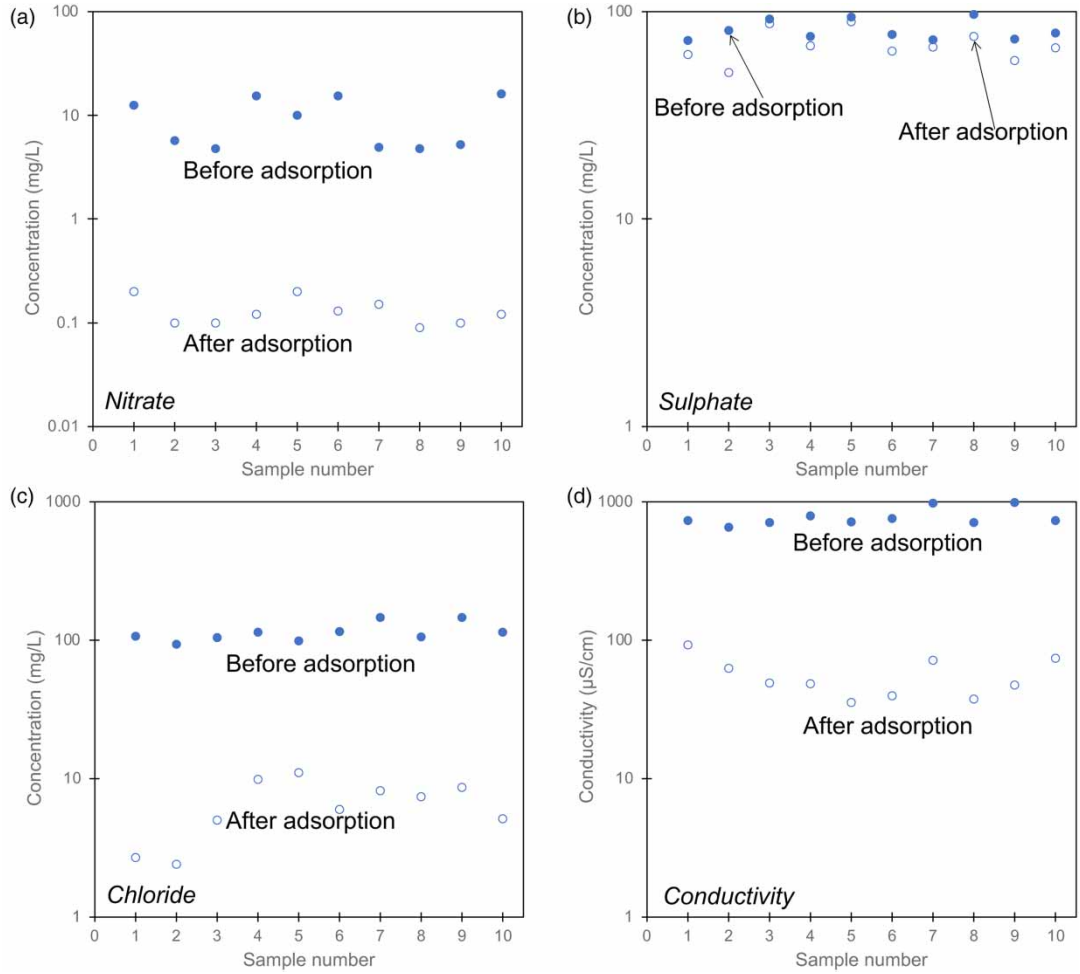

Figure 6 | Concentrations of (a) Nitrate; (b) Sulphate; (c) Chloride; and (d) Conductivity in the 10 water samples before and after the adsorption. Dots are values before the adsorption, and circles are after the adsorption.

monovalent ion-exchange membrane plays an important role here, which prevents most of the divalent ions from entering the membranes (Figure 3(b)). Therefore, the more important factor that ensures the full adsorption of the nitrate ions is increasing the salt adsorption capacity of the porous carbon materials, either by increasing the thickness of the electrode region (Porada *et al.* 2012), by employing porous electrode materials with higher capacity (Cohen *et al.* 2011; Porada *et al.* 2013; Yeh *et al.* 2015; Xu *et al.* 2016; Zhang *et al.* 2019; Gao *et al.* 2016), or by using an electrode material, which has a selective feature of nitrate ions over chloride ions (Oyarzun *et al.* 2019). In our case, using the current setup, given the experimental results, we are confident to apply our device to surface waters, which have a conductivity of less than 1,000 μS/cm.

3.4. Interference of ambient temperature

A common and inevitable drawback of LEDs is temperature shift, which means changing the ambient operational temperature may have an effect on the wavelength and the light strength of the LED leading to a higher error. Therefore, we tested the device at three different temperatures (10, 25, and 40 °C) in an environmental test chamber (JHY-H-408L, Moon Mountain, Xiamen, China). For each temperature, experiments were done at concentrations of 5, 10, 15, and 20 mg/L (Figure 7(a)) and the final result was calculated only using the calibration curve made at 25 °C. It is shown that most normalized values have an error within 10%, except for one data point at 10 °C, 5 mg/L (Figure 7(b)). It is suggested to operate the device under a relative stable temperature. In our next sections, all experiments were tested in the laboratory with a stable room temperature of around 25 °C and for the long-term experiment by the river, the device was installed in an apparatus cabinet with an air conditioner always set at 25 °C.

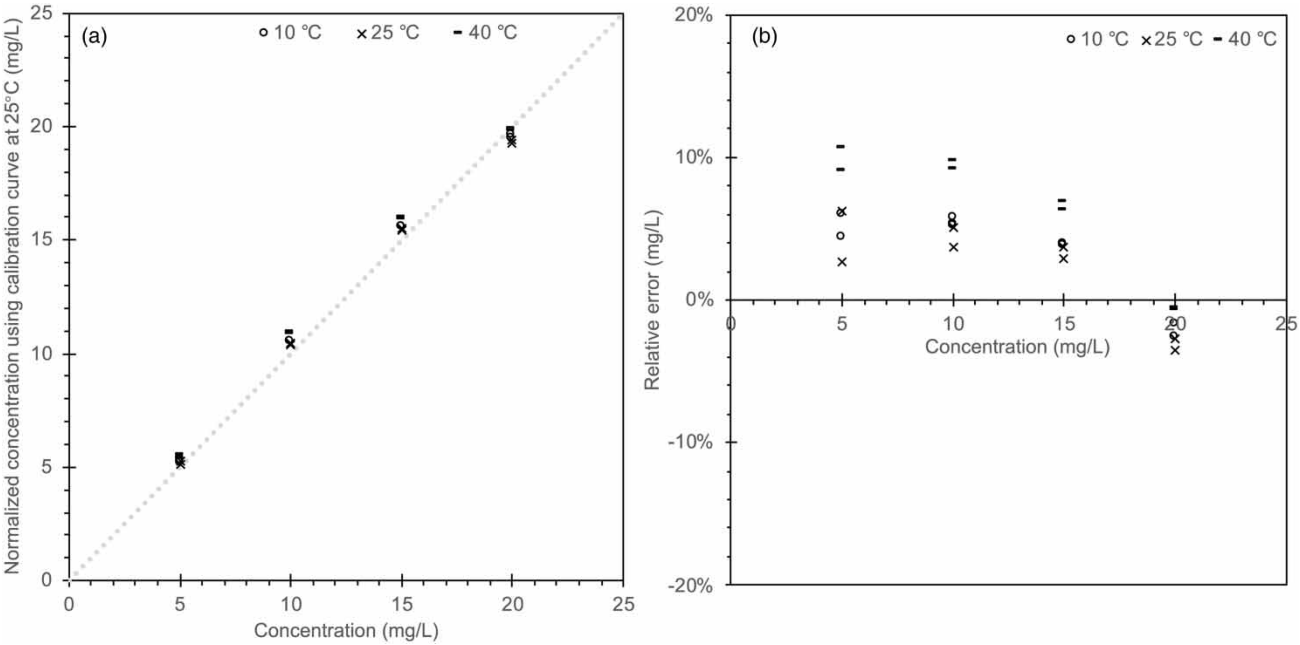

Figure 7 | (a) Concentration variation as a function of different temperature; and (b) Their relative error in comparison to the calibration curve at 25 °C. The dotted line is to guide the eyes, which ideally should cross all values.

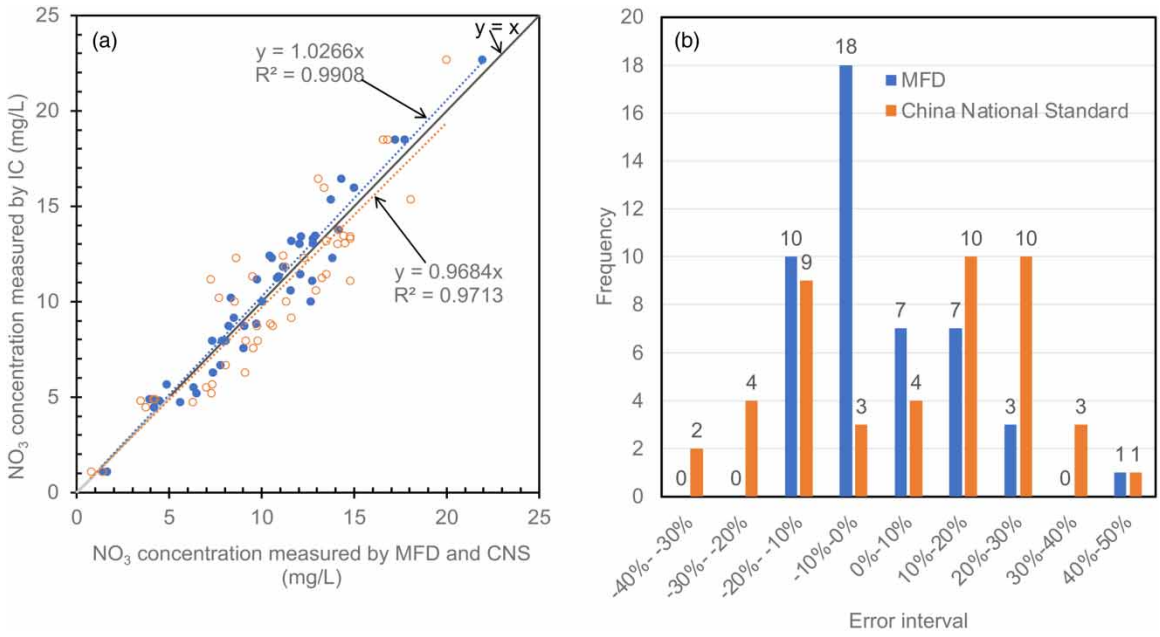

Figure 8 | (a) Correlation between the nitrate ion concentration measured by ion chromatography, microfluidic device (MFD) (dots), and the Chinese national standard method (open circles). The solid line connects the two angles is the ideal line ($y = x$) to guide the eyes. The dotted lines are the trend line generated by Excel; and (b) Histogram shows the frequencies as a function of error intervals of the two methods compared to the value measured by ion chromatography.

3.5. Verification by surface water samples

Forty-six surface water samples collected in the rivers in Shanghai are analyzed by the microfluidic device and the Chinese national standard method. Both results are compared with the values measured by the ion chromatography (Figure 8(a)).

For both groups of data, trend lines are generated by Excel, and the coefficients of determination (R^2) are given as well, which exhibits that the MCDI-MFD method has a higher correlation with the results obtained by ion chromatography that are used as the benchmark. Relative errors of the two methods compared to the integrated circuit (IC) values are shown in the histogram (Figure 8(b)). Likewise, the MCDI-MFD method also shows a better distribution over the error interval sections, where the majority is within the range of −20–20%. Whereas for the China National Standards (CNS) method, a big portion is within the range of −20 to 30%. Given its better performance in terms of accuracy compared to the CNS method, it is suggested that the MCDI-MFD can serve as a sufficient prewarning means for the online measurement of the nitrate concentration's trend in the surface waters.

3.6. Deployment in river

After having the device calibrated in the laboratory, we installed it in a river on downstream of a wastewater treatment plant discharge point deliberately in order to witness more variation in the nitrate concentration. The location of this installation is

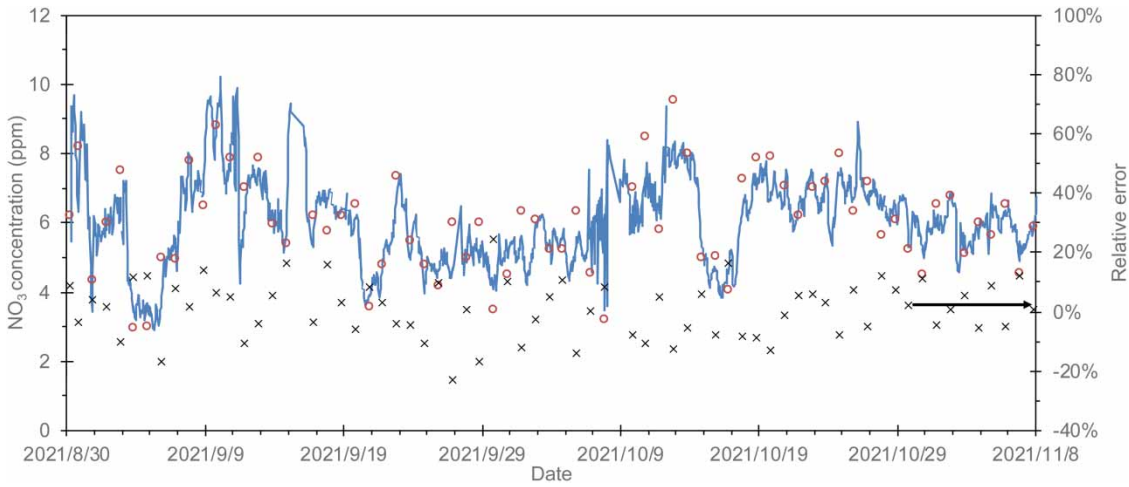

Figure 9 | NO_3 concentration change as a function of time in a river between 2021/8/30 and 2021/11/8. The solid line is values obtained by the MFD, the circles are samples analyzed by the ion chromatography in the lab, and the crosses are the relative errors between the MFD values and the lab analyzed values.

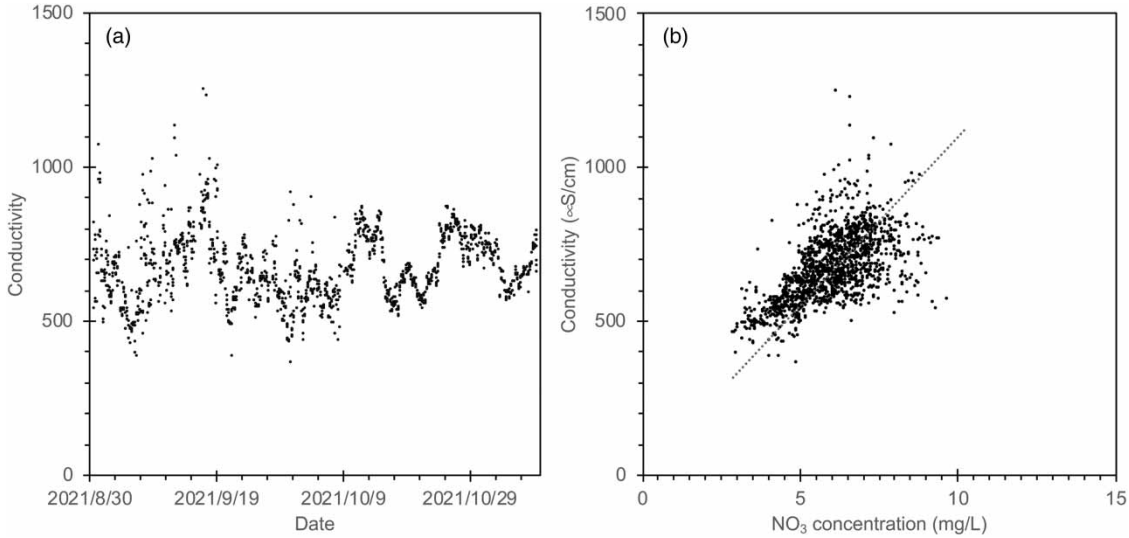

Figure 10 | (a) Conductivity change as a function of time in a river between 2021/8/30 and 2021/11/8. (b) Conductivity as a function of measured NO_3 concentration. The dotted line is the corresponding regression curve.

not permitted to be unveiled. The device was deployed from the end of August to the beginning of November 2021. This sensor was installed together with a pretreatment unit (Haoli Tech, Shanghai, China). This unit consists of a ceramic microfiltration membrane module and a water reservoir. The ceramic microfiltration membrane has an average pore size of 0.16 micrometer, which filters the water every 1 h. The filtered water was then pumped into the reservoir, where, the measurement starts, the sample was taken by the MFD. After the measurement, the back-wash process will start, and pressurized air is used to clean the membrane. Every day at 9 O'clock in the morning, one sample was taken from the water reservoir to be measured in the laboratory by ion chromatography.

During the two-month deployment, over 1,200 river water samples were measured. Our data and the values analyzed in the laboratory are in very good agreement. The relative errors are mostly in the range between −20 and 20% (Figure 9). Figure 10(a) shows the conductivity change during this period, which was mainly fluctuating between 500 and 1,000 μS/cm, and Figure 10(b) shows that the conductivity had a positive impact on the nitrate concentration. It is proven that this technology can be used directly as a means to monitor the trend of the nitrate concentration change in surface water in the Shanghai area with a relatively low conductivity below 1,000 μS/cm.

4. CONCLUSIONS

In this work, we investigated a novel method for the detection of nitrate concentrations in surface water using a miniaturized MCDI cell in combination with a microfluidic device. The MCDI cell was used for the separation of natural organic compounds and the nitrate ions prior to the determination of nitrate concentration by a 235-nm LED. It is shown that during the separation step, the optimal parameter setting (600 s charging time and 0.5 V cell potential) can lead to thorough adsorption of the nitrate ions, while most natural organic matters are left in the spacer channel. As a result, this new method can measure the nitrate concentration more accurately and directly using the 235-nm LED compared to the method adopted by the Chinese national standard. The measuring range of nitrate ions of our equipment is set at 0–20 mg/L, which can meet the detection requirements of nitrate in surface water in most cases. The long-term study shows that this online equipment can be used to monitor the trend of the nitrate concentration variation in surface water with conductivity lower than 1,000 μS/cm in the world and the data show an excellent agreement with the lab-analyzed values.

ACKNOWLEDGEMENTS

This work was supported by the horizontal project between Shanghai Bozhongguanche Intelligent Technology Co., Ltd (Haoli Technology®) and East China Normal University (project number: 2020KFR0257).

DATA AVAILABILITY STATEMENT

All relevant data are included in the paper or its Supplementary Information.

CONFLICT OF INTEREST

The authors declare there is no conflict.

REFERENCES

Aoki, T., Fukuda, S., Hosoi, Y. & Mukai, H. 1997 Rapid flow injection analysis method for successive determination of ammonia, nitrite, and nitrate in water by gas-phase chemiluminescence. *Anal. Chim. Acta.* **349**, 11–16. https://doi.org/10.1016/S0003-2670(97)00273-0.

Baird, R. B., Eaton, A. D., Rice, E. W. & Bridgewater, L. 2017 *Standard Methods for the Examination of Water and Wastewater (Vol. 23)*. American Public Health Association, Washington, DC.

Beaton, A. D., Cardwell, C. L., Thomas, R. S., Sieben, V. J., Legiret, F. E., Waugh, E. M., Statham, P. J., Mowlem, M. C. & Morgan, H. 2012 Lab-on-chip measurement of nitrate and nitrite for in situ analysis of natural waters. *Environ. Sci. Technol.* **46**, 9548–9556. https://doi.org/10.1021/es300419u.

Burt, T. P., Howden, N. J. K., Worrall, F. & Whelan, M. J. 2010 Long-term monitoring of river water nitrate: how much data do we need? *J. Environ. Monit.* **12**, 71–79. https://doi.org/10.1039/B913003A.

Cerón, M. R., Aydin, F., Hawks, S. A., Oyarzun, D. I., Loeb, C. K., Deinhart, A., Zhan, C., Pham, T. A., Stadermann, M. & Campbell, P. G. 2020 Cation selectivity in capacitive deionization: elucidating the role of pore size, electrode potential, and ion dehydration. *ACS Appl. Mater. Interfaces.* **12**, 42644–42652. https://doi.org/10.1021/acsami.0c07903.

Cogan, D., Cleary, J., Phelan, T., McNamara, E., Bowkett, M. & Diamond, D. 2013 Integrated flow analysis platform for the direct detection of nitrate in water using a simplified chromotropic acid method. *Anal. Methods.* **5**, 4798–4804. https://doi.org/10.1039/c3ay41098f.

Cohen, I., Avraham, E., Noked, M., Soffer, A. & Aurbach, D. 2011 Enhanced charge efficiency in capacitive deionization achieved by surface-treated electrodes and by means of a third electrode. *J. Phys. Chem. C.* **115**, 19856–19863. https://doi.org/10.1021/jp206956a.

Costa, A. S., Passos, E. D. A., Garcia, C. A. B. & Alves, J. D. P. H. 2011 Characterization of dissolved organic matter in the piauí river estuary, northeast Brazil. *J. Braz. Chem. Soc.* **22**, 2139–2147. https://doi.org/10.1590/S0103-50532011001100017.

Cotruvo, J., Fawell, J. K., Giddings, M., Jackon, P., Magara, Y., Festo Ngowi, A. V. & Ohanian, E. 2011 *Nitrate and Nitrite in Drinking-Water*. https://doi.org/10.1108/eb058626.

Davis, J., Moorcroft, M. J., Wilkins, S. J., Compton, R. G. & Cardosi, M. F. 2000 Electrochemical detection of nitrate and nitrite at a copper modified electrode. *Analyst.* **125**, 737–741. https://doi.org/10.1039/a909762g.

Divyapriya, G., Vijayakumar, K. K. & Nambi, I. 2019 Development of a novel graphene/CO_3O_4 composite for hybrid capacitive deionization system. *Desalination.* **451**, 102–110. https://doi.org/10.1016/j.desal.2018.03.023.

Gal, C., Frenzel, W. & Möller, J. 2004 Re-examination of the cadmium reduction method and optimisation of conditions for the determination of nitrate by flow injection analysis. *Microchim. Acta.* **146**, 155–164. https://doi.org/10.1007/s00604-004-0193-7.

Gao, X., Porada, S., Omosebi, A., Liu, K., Biesheuvel, P. M. & Landon, J. 2016 Complementary surface charge for enhanced capacitive deionization. *Water Res.* **92**, 275–282. https://doi.org/http://dx.doi.org/10.1016/j.watres.2016.01.048.

Hong, S. P., Yoon, H., Lee, J., Kim, C., Kim, S., Lee, J., Lee, C. & Yoon, J. 2020 Selective phosphate removal using layered double hydroxide/reduced graphene oxide (LDH/rGO) composite electrode in capacitive deionization. *J. Colloid Interface Sci.* **564**, 1–7. https://doi.org/10.1016/j.jcis.2019.12.068.

Kaniansky, D., Zelenský, I., Hybenová, A. & Onuska, F. I. 1994 Determination of chloride, nitrate, sulfate, nitrite, fluoride, and phosphate by on-line coupled capillary isotachophoresis-capillary zone electrophoresis with conductivity detection. *Anal. Chem.* **66**, 4258–4264. https://doi.org/10.1021/ac00095a022.

Klučáková, M. 2018 Size and charge evaluation of standard humic and fulvic acids as crucial factors to determine their environmental behavior and impact. *Front. Chem.* **6**, 1–8. https://doi.org/10.3389/fchem.2018.00235.

Li, Z., Mao, S., Yang, Y., Sun, Z. & Zhao, R. 2021 Controllable synthesis of a hollow core-shell Co-Fe layered double hydroxide derived from Co-MOF and its application in capacitive deionization. *J. Colloid Interface Sci.* **585**, 85–94. https://doi.org/10.1016/j.jcis.2020.11.091.

Ma, J., Cheng, Y., Wang, L., Dai, X. & Yu, F. 2020 Free-standing Ti3C2Tx MXene film as binder-free electrode in capacitive deionization with an ultrahigh desalination capacity. *Chem. Eng. J.* **384**, 123329. https://doi.org/10.1016/j.cej.2019.123329.

MacFarlane, R. B. 1978 Molecular weight distribution of humic and fulvic acids of sediments from a north Florida estuary. *Geochim. Cosmochim. Acta.* **42**, 1579–1582. https://doi.org/10.1016/0016-7037(78)90028-5.

Moorcroft, M. J., Davis, J. & Compton, R. G. 2001 Detection and determination of nitrate ions: a review. *Talanta.* **54**, 785–803. www.elsevier.com/locate/talanta.

Mubita, T. M., Dykstra, J. E., Biesheuvel, P. M., van der Wal, A. & Porada, S. 2019 Selective adsorption of nitrate over chloride in microporous carbons. *Water Res.* **164**, 114885. https://doi.org/10.1016/j.watres.2019.114885.

National Environmental Protection Bureau (NEPB) 2007 *Water Quality-Determination of Nitrate-Nitrogen-Ultraviolet Spectrophotometry HJ/T 346-2007*. Beijing.

Nightingale, A. M., Hassan, S. U., Warren, B. M., Makris, K., Evans, G. W. H., Papadopoulou, E., Coleman, S. & Niu, X. 2019 A droplet microfluidic-based sensor for simultaneous in situ monitoring of nitrate and nitrite in natural waters. *Environ. Sci. Technol.* **53**, 9677–9685. https://doi.org/10.1021/acs.est.9b01032.

Noonan, O., Liu, Y., Huang, X. & Yu, C. 2018 Layered graphene/mesoporous carbon heterostructures with improved mesopore accessibility for high performance capacitive deionization. *J. Mater. Chem. A.* **6**, 14272–14280. https://doi.org/10.1039/c8ta03114b.

Ogilvie, I. R. G., Sieben, V. J., Floquet, C. F. A., Zmijan, R., Mowlem, M. C. & Morgan, H. 2010 Reduction of surface roughness for optical quality microfluidic devices in PMMA and COC. *J. Micromech. Microeng.* **20**. https://doi.org/10.1088/0960-1317/20/6/065016.

Oyarzun, D. I., Pham, T. A., Zhan, C., Hawks, S. A., Cero, M. R., Loeb, C. K., Mew, D., Deinhart, A., Wood, B. C., Santiago, J. G., Stadermann, M. & Campbell, P. G. 2019 Using ultramicroporous carbon for the selective removal of nitrate with capacitive deionization. https://doi.org/10.1021/acs.est.9b01374.

Peng, W., Wang, W., Han, G., Huang, Y. & Zhang, Y. 2020 Fabrication of 3D flower-like MoS2/graphene composite as high-performance electrode for capacitive deionization. *Desalination.* **473**, 114191. https://doi.org/10.1016/j.desal.2019.114191.

Porada, S., Bryjak, M., Van Der Wal, A. & Biesheuvel, P. M. 2012 Effect of electrode thickness variation on operation of capacitive deionization. *Electrochim. Acta.* **75**, 148–156. https://doi.org/10.1016/j.electacta.2012.04.083.

Porada, S., Zhao, R., van der Wal, A., Presser, V. & Biesheuvel, P. M. 2013 Review on the science and technology of water desalination by capacitive deionization. *Prog. Mater. Sci.* https://doi.org/http://dx.doi.org/10.1016/j.pmatsci.2013.03.005.

Porada, S., Zhao, R., van der Wal, A., Presser, V. & Biesheuvel, P. M. n.d. Review on the science and technology of water desalination by capacitive deionization. *Prog. Mater. Sci.* https://doi.org/http://dx.doi.org/10.1016/j.pmatsci.2013.03.005.

Rodrigues, A., Brito, A., Janknecht, P., Proena, M. F. & Nogueira, R. 2009 Quantification of humic acids in surface water: effects of divalent cations, pH, and filtration. *J. Environ. Monit.* **11**, 377–382. https://doi.org/10.1039/b811942b.

Thurman, E. M., Wershaw, R. L., Malcolm, R. L. & Pinckney, D. J. 1982 Molecular size of aquatic humic substances. *Org. Geochem.* **4**, 27–35. https://doi.org/10.1016/0146-6380(82)90005-5.

Xu, X., Liu, Y., Wang, M., Zhu, C., Lu, T., Zhao, R. & Pan, L. 2016 Hierarchical hybrids with microporous carbon spheres decorated three-dimensional graphene frameworks for capacitive applications in supercapacitor and deionization. *Electrochim. Acta.* **193**, 88–95. https://doi.org/http://dx.doi.org/10.1016/j.electacta.2016.02.049.

Xu, X., Yang, T., Zhang, Q., Xia, W., Ding, Z., Eid, K., Abdullah, A. M., Shahriar, M., Hossain, A., Zhang, S., Tang, J., Pan, L. & Yamauchi, Y. 2020 Ultrahigh capacitive deionization performance by 3D interconnected MOF-derived nitrogen-doped carbon tubes. *Chem. Eng. J.* **390**, 124493. https://doi.org/10.1016/j.cej.2020.124493.

Yeh, C.-L., Hsi, H.-C., Li, K.-C. & Hou, C.-H. 2015 Improved performance in capacitive deionization of activated carbon electrodes with a tunable mesopore and micropore ratio. *Desalination.* **367**, 60–68. https://doi.org/http://dx.doi.org/10.1016/j.desal.2015.03.035.

Yu, G., Wang, J., Liu, L., Li, Y., Zhang, Y. & Wang, S. 2020 The analysis of groundwater nitrate pollution and health risk assessment in rural areas of Yantai, China. *BMC Public Health.* **20**, 437. https://doi.org/10.1186/s12889-020-08583-y.

Zhang, Y., Chen, L., Mao, S., Sun, Z., Song, Y. & Zhao, R. 2019 Fabrication of porous graphene electrodes via CO_2 activation for the enhancement of capacitive deionization. *J. Colloid Interface Sci.* **536**. https://doi.org/10.1016/j.jcis.2018.10.063.

First received 6 May 2022; accepted in revised form 30 January 2023. Available online 8 February 2023